

Abstract

The Agulhas leakage to the South Atlantic (SA) exhibits strong anti-correlations with the mass flux of the Agulhas Current. This is accompanied by the migration of the Agulhas retroflexion whose normal position (NPR) is near Cape Agulhas, where the slant of the South African coast is very small. During periods of strong incoming flux (SIF), the retroflexion shifts upstream to Port Elizabeth or East London, where the coastline shape has a “kink”, i.e., the slant changes abruptly from small on the west side, to large (about 55°) on the east side. Here, we show that the variability of rings shedding maybe attributed to this kink.

To do so, we develop a nonlinear analytical model for retroflexion near a coastline that consists of two sections, one strongly slanted (corresponding to the east side) and the other zonal (corresponding to the west side). The principal difference between this and the model of a single straight slanted coast discussed in our earlier papers is that a free purely westward propagation of eddies along the zonal coastline section is allowed in the kinked case. This introduces the interesting situation where the strong slant of the coast east of the kink prohibits the formation and shedding of rings whereas the coast west of the kink encourages such shedding. Therefore, the kink model “locks” the position of the retroflexion forcing it to occur just downstream of the kink. That is, rings are necessarily shed from the retroflexion area in our kinked model, regardless of the eastern coast slant. By contrast, the application of “no-kink” model for an “averaged” slant (at the same point as the kink) leads to the conclusion that shedding is almost completely arrested by the slant.

We suggest that the difference between the intensities of rings shedding during NPR and SIF is due to the shift in the zero curl line in respect to the kink. When the zero curl intersects the coast north of the kink the transport is small but it is large when the zero curl is situated south of the kink. Simple process-oriented numerical simulations are in fair agreement with our results.

Retroflexion from a double slanted coastline for Agulhas leakage variability

V. Zharkov et al.

Title Page

Abstract

Introduction

Conclusions

References

Tables

Figures

⏪

⏩

◀

▶

Back

Close

Full Screen / Esc

Printer-friendly Version

Interactive Discussion



1 Introduction

This article supplements our recent theoretical investigations suggesting that Agulhas ring shedding variability is primarily due to the inertial and momentum imbalances, and the manner that they combine with the coastal slant near the retroflexion (Zharkov and Nof, 2008a, ZNab, hereafter). Here, we push our recent work closer to reality by introducing a “kink” to the previously straight coastline configuration. This allows us to mimic the coastline slant better by fitting the new model, in which the land can now be either convex or concave, more closely to it. In a (land) concave model the land bulges toward the ocean so that the ocean occupies more than half of the 360° plane whereas in the convex model, the ocean bulges into the land so that it occupies less than half the 360° plane. (The former is applicable to the South African Continent whereas the latter is more appropriate to the Southwest Atlantic, which is not our focus here.)

In the South African case, the normal position of retroflexion (NPR) of the Agulhas Current (AC) is to the southwest of Cape Agulhas (Lutjeharms and van Ballegooyen, 1988a). However, occasionally, the retroflexion shifts upstream and occurs near Port Elizabeth or East London (Fig. 1, upper panel). Such unusual eastward shift occurs during periods of strong incoming flux (SIF). The geometries of the coastline near which the two different retroflexions occur are distinctly different. During SIF it occurs near a coastline that is strongly concave (i.e., the angle between the two straight coasts is considerably smaller than 180°, looking off-shore) whereas during NPR, it is weakly concave. Using both analytical and numerical models we show that this difference affects the production of eddies and, therefore, the leakage into the South Atlantic (SA). Namely, the coastal “kink” acts like a valve for the leak. In contrast to what our intuition suggests – that strong flows will be associated with strong leaks – the kink implies that smaller leaks occur during SIF rather than NPR, because, during the SIF, the retroflexion occurs north of the kink. We will show also that, for the SIF periods, the “kink” model gives significantly better results than the straight coast model in the sense that the difference between the predicted eddy mass flux and the observations

OSD

7, 1209–1244, 2010

Retroflexion from a double slanted coastline for Agulhas leakage variability

V. Zharkov et al.

Title Page

Abstract

Introduction

Conclusions

References

Tables

Figures



Back

Close

Full Screen / Esc

Printer-friendly Version

Interactive Discussion

Retroflexion from a double slanted coastline for Agulhas leakage variability

V. Zharkov et al.

Title Page

Abstract

Introduction

Conclusions

References

Tables

Figures

⏪

⏩

◀

▶

Back

Close

Full Screen / Esc

Printer-friendly Version

Interactive Discussion



is 3–4 times smaller. For NPR, the difference between the concave model and the straight coastline model is insignificant because the angle between the two almost straight coasts is very close to 180° . The main aspect of the kink model is that east of the kink the coastline slant is too high to allow the production of rings whereas the one on the west allows the production of rings. As a result, the production of rings is allowed in a manner that is quite different from that implied by the mean slant. More importantly, the kink locks the position of the retroflexion to just downstream of the kink.

1.1 Observational background

The position of the retroflected AC off shore is determined by the position of the zero wind stress curl (WSC). At the same time, the exact path and position of the AC retroflexion adjacent to the coastline is sensitive to various parameters such as the AC volume transport and the coastline orientation (see e.g., Lutjeharms and van Ballegooyen, 1984). During NPR, when the AC volume transport is low, the zero WSC is situated on the south side favoring the westward protrusion of Agulhas retroflexion. In the same time, there is an increase of warm water influx (via rings) into the SA. During SIF, on the other hand, the WSC shifts northward so that the retroflexion shifts eastward to a location where the coastline has a “kink” (i.e., the angle between the two, approximately straight, coastlines is considerably smaller than 180° – looking off-shore). This is consistent with the observation that rings in the Agulhas region are typically shed about 5–6 times per year, but the period of their formation increases sometimes to almost half-a-year (e.g., Byrne et al., 1995; Gordon et al., 1987; Lutjeharms, 2006; Schouten et al., 2000; van Aken et al., 2003). We shall suggest here that the difference is associated with the shifting of the retroflexion from a no-kink coastline to a coastline with a kink.

Interestingly, there is no consensus on the significance of seasonal variability to the retroflexion. Shannon (1985), and Esper et al. (2004) point to a seasonal variability of the retroflexion position, which is in agreement with the numerical calculations

Retroflection from a double slanted coastline for Agulhas leakage variability

V. Zharkov et al.

Title Page

Abstract

Introduction

Conclusions

References

Tables

Figures

⏪

⏩

◀

▶

Back

Close

Full Screen / Esc

Printer-friendly Version

Interactive Discussion

of Reason et al. (2003) suggesting that the incoming flux is maximal in winter and minimal in summer. Field et al. (1997) also point to seasonal variation in the Agulhas volume transport, and some seasonality in the Agulhas SSH was also shown by Matano et al. (1998). Goni et al. (1997) suggest that seasonality can very moderately affect ring shedding. Their observations during 1992–1995 suggest that six out of the 17 consecutive Agulhas rings were first observed in austral summers, and only four rings in winters. In addition, the volumes of all four winter-rings were less than the average value. However, such variations are not commonly believed to be responsible for significant seasonal modifications of the ring's shedding regime (e.g., van Sebille, 2009).

In contrast to the above ideas of seasonality, Lutjeharms and van Balle-gooyen (1988b), and Lutjeharms (2006) speak about anomalous and occasional eastward shift of the Agulhas retroflection area. Associated with these shifts is a decrease in ring shedding. The anomalous eastward migration of Agulhas retroflection occurs usually 2–3 times per year and lasts 3–6 weeks. There were also observations of very irregular, inter-annual variations of the retroflection position. For instance, the so-called “early retroflection” events occurred in 1986 (Shannon et al., 1990) and 2000–2001 (Quartly and Srokosz, 2002; de Ruijter et al., 2004) when the AC retroflected to the east of the Agulhas Plateau. During the second “early retroflection” (i.e., 2000–2001), no eddies were shed for about five months.

De Ruijter et al. (2004) suggest that the strong reduction (or even shutoff) of the leakage via rings is due to La-Niña. By contrast, during El-Niños, enhancing leakage occurs. This is seen in Fig. 5 of van Sebille et al. (2009b) where the decrease in Agulhas leakage in 1986 (during the first known “early retroflection”) is clearly noted. We can expect the time periods between consecutive “La-Niñas” events to be comparable to the classic ENSO periods but with no regularity. (Note that in Biastoch et al., 2008, they are two years apart.) These events in the Indian Ocean and the AC are much shorter than the usual La-Niña conditions in the Pacific (see e.g., van Sebille et al., 2009a, VS, hereafter).

1.2 Theoretical background

An anti-correlation between the AC transport and the westward protrusion of the retroflexion (and, therefore, increase in Agulhas leakage) was first pointed out by de Ruijter and Boudra (1985), Boudra and Chassignet (1988), Esper et al. (2004), and van Sebille et al. (2009a). Also, it was shown that the position of Agulhas retroflexion has a strong impact on the inter-annual variations of the inflow to the South Atlantic, which, in turn, significantly affects the decadal variability in the Atlantic MOC (Weijer et al., 1999; Weijer et al., 2002; Biastoch et al., 2008). While all of these studies are informative, none specifically addressed the dynamics involved in the anti-correlation. The idea that coastal geometry is important to retroflexing currents is also not new. It was recognized by Ou and de Ruijter (1986), Boudra and Chassignet (1988), de Ruijter et al. (1999), Chassignet and Boudra (1988), and Pichevin et al. (1999) though none specifically focused on the issue that we are addressing here where a small slant allows for stronger eddies production.

Of these, the study of Ou and de Ruijter (1986) is the closest to our new kink model and it is, therefore, elaborated on below. Ou and de Ruijter (1986) assumed that the flow has a scale larger than the Rossby radius, and that that scale is also larger than the continental radius of curvature. In their model, the AC attempts to follow the coastline but cannot continue to do so when the coastline curves strongly to the right (looking downstream) because the curving is too sharp for the current to mimic. Consequently, the continent separates from the current and a space opens up between the continent and the current. In its unsuccessful attempt to continue hugging the continent, the current cyclonically loops upon itself in this open space. Supposedly, this looping produces the retroflexing eddies. The main weakness of this appealing theory is that it produces eddies of the wrong sign. Ou and de Ruijter (1986) eddies are cyclonic whereas the retroflexion eddies are anticyclonic leading one to question the proposed process.

Retroflexion from a double slanted coastline for Agulhas leakage variability

V. Zharkov et al.

Title Page

Abstract

Introduction

Conclusions

References

Tables

Figures



Back

Close

Full Screen / Esc

Printer-friendly Version

Interactive Discussion



2 Statement of problem

As in ZNab, we consider a boundary current (with density ρ) embedded in an infinitely deep, stagnant lower layer (whose density is $\rho + \Delta\rho$), except that, here, the vertical boundary on the west is not a single straight line. The first coastline to be considered (Concave I) consists of two rectilinear sections one of them is zonal, and the second one is slanted (Fig. 3) at an angle that varies between 0° and 90° . The current flows southwestward along the slanted section and then retroflects, south of the kink.

As mentioned, the main differences between the case considered here and the no-kink model considered in ZNab are: (i) here, the rings escape from the generation area faster than in the no-kink case (because they no longer run into the wall) implying a larger production of rings, and (ii) here, the upstream momentum-flux zonal component is smaller leading to a smaller production of eddies. Which of the two competing processes dominates depends on the problem particular conditions. In all the cases that we looked at, the first processes dominated. Note that the appropriate momentum-flux to consider here is the zonal one (not the slanted), because the rings are generated just downstream of the kink and start migrating westward right away. The numerics will later verify this assessment. Using the same notation used by ZNab (reproduced in our Table A1), one ultimately finds the following equation for the ring radius R as a function of time,

$$\begin{aligned} & \frac{(\alpha f_0)^3}{240} \left[2(1 + \cos\gamma)R^5 - 5(\delta_1^2 - \delta_2^2)R^3 - 5(\delta_1^3 \cos\gamma + \delta_2^3)R^2 \right. \\ & \left. + (3\delta_1^5 \cos\gamma + 5\delta_1^2 \delta_2^3 - 2\delta_2^5) \right] + \frac{\alpha^2 f_0 g' h_0}{12} \left[(1 + \cos\gamma)R^3 - (\delta_1^3 \cos\gamma + \delta_2^3) \right] \\ & - \pi R^2 \left[g'H + \frac{\alpha(2 - \alpha)f_0^2 R^2}{16} \right] \frac{dR}{dt} = 0. \end{aligned} \quad (1)$$

Retroflection from a double slanted coastline for Agulhas leakage variability

V. Zharkov et al.

Title Page

Abstract

Introduction

Conclusions

References

Tables

Figures

◀

▶

◀

▶

Back

Close

Full Screen / Esc

Printer-friendly Version

Interactive Discussion



This equation differs from its counterpart in ZNa in the sense that the terms with $\alpha\beta R^2$ are absent here, and that $\cos\gamma$ serves as multiplier for other terms than in ZNa. The remaining equations are the same as in ZNa and are not reproduced here.

3 Solution

5 We solved the system of equations, again by using the Runge-Kutta method of the fourth order. We used: $Q=70$ Sv; $g'=2\times 10^{-2}$ ms⁻²; $f=8.8\times 10^{-5}$ s⁻¹ (corresponding to 35° of latitude) and, we took zero and 300 m for h_0 . The parameters α and γ were varied between 0.1 and 1.0, and between 0° and 90°, respectively. The functions $R(t)$ and $\Phi(t)$, in the case of zero PV ($\alpha=1$), $h_0=300$ m, and $\beta=2.3\times 10^{-11}$ m⁻¹ s⁻¹ are shown in Fig. 4 (upper and lower panels). For a comparison, the right panels in Fig. 4 show the analogous plots for the ZNa, ZNb model (without triangles and squares). The quantitative difference between the two models is obvious. Only the curves for $\gamma=0$ are identical because the case of zonal wall is the same for both models. The $\Phi(t)$ curves approach asymptotic values that decrease with growing γ . As expected, in the case of a zonal wall ($\gamma=0$), the asymptotic value is close to 4/3. All the curves for $\gamma<60^\circ$ intersect the “dead line” $\Phi=1$, indicating that the ‘vorticity paradox’ occurs above this line. We can see that the paradox could be circumvented only for $\gamma\geq 60^\circ$ (instead of $\gamma\geq 15^\circ$ in the ZNa model), because it is for this minimal value of γ that Φ does not intersect the deadline. The asymptotic value for $\gamma=90^\circ$ is close to 2/3 indicating that this case is similar to the ballooning of outflows problem (Nof and Pichevin, 2001).

15 For smaller values of α , the curves of $R(t)$ and $\Phi(t)$ are similar to those shown in Fig. 4 but the asymptotical values of Φ go down with decreasing α . They can be approximated by $2\alpha(1+\cos\gamma)/(1+2\alpha)$, implying that the detached rings compensate for the momentum of both the entire retroflected current and the zonal projection of the incoming current. Therefore, the “vorticity paradox” is circumvented when the slant of the tilted coastline section is not less than $\cos^{-1}(1/2\alpha)$, which is 60° for zero PV ($\alpha=1$).

Retroflection from a double slanted coastline for Agulhas leakage variability

V. Zharkov et al.

Title Page

Abstract

Introduction

Conclusions

References

Tables

Figures

⏪

⏩

◀

▶

Back

Close

Full Screen / Esc

Printer-friendly Version

Interactive Discussion



4 Detachment of rings

4.1 “Lower” and “upper” boundaries

Following ZNb, the generation period for each individual ring is,

$$t_f = (2R_f + d)/|C_{xf}|, \quad (2)$$

5 where d is the distance between two consecutive rings, C_x is the ring propagation rate and the subscript f denotes the “final” value. The “lower boundary” for the final eddy size (R_{fl}) is obtained from the condition of “kissing eddies”, i.e., $d=0$.

Next, we define the “upper boundary” (R_{fu}) for the final BE size, and t_{fu} for the generation period. This implies that the ring can propagate at least its own diameter,

$$10 \int_0^{t_{fu}} |C_x| dt = 2 R_{fu}. \quad (3)$$

Physically, the “upper boundary” corresponds more directly to the detachment of rings, whereas the “lower boundary” is a condition for the eddy chain formation. So, rings detach and propagate out of the retroflection area only when R_{fl} is indeed less than R_{fu} .

15 4.2 Analysis of “lower” and “upper” boundaries

Here, we shall use $2.3 \times 10^{-11} \text{ m}^{-1} \text{ s}^{-1}$ and $6 \times 10^{-11} \text{ m}^{-1} \text{ s}^{-1}$ for β . The first is common whereas the second is magnified (more convenient for the runs). The left upper panel of Fig. 5 shows R_{fl} and R_{fu} as functions of γ , whereas the right panel shows the analogous figure for the no-kink model. It is seen that, for both models, the functions decrease as γ grows. However, in the Concave I case, the curves of R_{fl} and R_{fu} do not intersect, implying that there is no critical slant angle. We see that the distance between the lower and upper boundaries decreases slightly with diminishing α . On

Retroflection from a double slanted coastline for Agulhas leakage variability

V. Zharkov et al.

Title Page

Abstract

Introduction

Conclusions

References

Tables

Figures

◀

▶

◀

▶

Back

Close

Full Screen / Esc

Printer-friendly Version

Interactive Discussion



the contrary, in the ZNb model, the lower and upper boundaries do intersect, and such critical points are circled here. (When the slant is “super-critical”, the rings do not move out of the retroflection area fast enough and, consequently, they are re-captured by the flow behind.) In addition, in the ZNb model, the curves for $\alpha=1$ terminate much earlier than for $\gamma=90^\circ$ because, for large γ and small α , the BE is forced into the wall instead of growing. Such a process does not occur in the Concave I model considered here.

The second and third panels in Fig. 5 show the periods of ring detachment and the detached eddies propagation rates. It is seen that the detachment period decreases with growing α in the same way that the final eddy radius does. Here, we again see no intersection or convergence of the curves depicting upper and lower boundaries (i.e., no critical angle). In addition, we see another difference with the analogous figures in ZNb model (right panels), where t_{fl} and t_{fu} tend to infinity, and $C_{\xi l}$ and $C_{\xi u}$ go to zero when $\gamma \rightarrow 90^\circ$. This is the case because, when the retroflection occurs near the kink, detached eddies can now (Concave I) propagate westwards with no obstacles.

4.3 The mass flux going into rings

We will now estimate the ratio of mass flux going into the growth of the rings to the incoming flux. Because Φ depends on time, this is obtained by averaging instant values over the period of eddy generation. The bottom panels in Fig. 5 show Φ versus γ for different values of α . Also, the right panel shows the analogous plot for the ZNb model. As expected, averaged values of Φ decrease with γ . It is seen that Φ_u and Φ_l as functions of γ (corresponding to the same value of α) do not intersect, in contrary with ZNb (bottom right), where they intersect each other at first at the points corresponding to γ between 4° and 35° , and then re-intersect when the angle is critical (and $\alpha > 0.1$). Note that the starting values of Φ are above the “dead line” (meaning appearance of the “vorticity paradox”) for $\alpha > 0.8$. For the maximal values, corresponding to $\alpha = 1$, they are considerably less than $4/3$, because the instant values of Φ are much less than 1 at the beginning of eddy development. For $\gamma > 34^\circ$, all the curves are below the dead line.

The main differences with ZNb are the same as those mentioned above – no critical angles, and Φ does not tend to zero with growing γ .

Although not discussed above, one can show that varying upper layer thickness has very weak influence on the detached rings. Using the modified value of β does not lead to qualitative differences, either. However, the propagation rate of rings increases, and the generation period decreases. Also, the lower and upper boundaries become close to each other, meaning that, for large γ , the shedding regime is nearly critical but not supercritical.

5 Numerical simulations

As in our previous studies, we used a modified version of the Bleck and Boudra (1986) reduced gravity isopycnic model with a passive lower layer and employed the Orlanski (1976) second-order radiation conditions for the open boundary. The basin size was taken to be $3200 \times 1600 \text{ km}^2$. The continent was modeled by one fixed meridional wall (600 km long), one zonal wall that could be either 2200 km (in the case $\gamma=0$) or 1000–1200 km long, and, for $\gamma>0$, a wall inclined by the angle γ to the zonal direction (γ varied between 15° and 90° in steps of 15°). The walls were taken to be slippery.

The experiment began by turning on an outflow at $t=0$; the numerical source was an open channel containing streamlines parallel to the slanted wall in the incoming current and horizontal in the outgoing flow. The initial velocity profile across the channel was linear, and the thickness profile was parabolic. Because each run provides many data points, it is believed that we have enough data to work with. We chose the initial PV of outflows so that the starting value of α was 0.1, 0.4, and 1.0. We note here that, as expected, at the beginning of each run when the orbital velocities were still high, α changed relatively quickly.

The numerical parameters were: (i) a time step of 120 s; (ii) a grid step of 20 km; (iii) a Laplacian viscosity coefficient $\nu=700 \text{ m}^2 \text{ s}^{-1}$ for $\gamma>15^\circ$ and for $\gamma=15^\circ$, $\alpha>0.1$; $1000 \text{ m}^2 \text{ s}^{-1}$ for $\gamma=15^\circ$, $\alpha=0.1$; and $1800 \text{ m}^2 \text{ s}^{-1}$ for the purely zonal wall case. Other

Retroflection from a double slanted coastline for Agulhas leakage variability

V. Zharkov et al.

Title Page

Abstract

Introduction

Conclusions

References

Tables

Figures

⏪

⏩

◀

▶

Back

Close

Full Screen / Esc

Printer-friendly Version

Interactive Discussion



that such rings form and detach even earlier than the BE does, and propagate into the retroreflection area, forcing the BE to detach as well (not shown).

Note that, in some cases, rings' shedding was completely prevented by re-capturing (as in the super-critical case for the retroreflection from straightforward slanted coast), a mechanism not included in the retroreflection paradox calculations (Nof and Pichevin, 1996). It is worth mentioning here in passing that Pichevin et al. (1999) suggest that, according to their simulations, upstream rings formed off-shore (in the northeastern part of the retroflected current) detach, and ultimately re-encounter the approaching current. They supposed that these events were artificial, suggesting that, in nature, such eddies are observed to be advected eastward. However, Lutjeharms (2006, p. 227) notes that at least cold cyclonic eddies (formed in the Agulhas Return Current) propagate westward and are subsequently absorbed by the first meander located in their westward paths.

We also quantitatively compared the model with the numerics. The results are similar to those mentioned in ZNb, i.e., the agreement in rings radii is good, with possible difference of about 20%, on average. However, the propagation rates are on average about half in the numerics than in our model, again because of the effect of viscosity.

6 Agulhas rings leakage variability

Before presenting the variability analysis, we remind the reader that our purpose here is not to duplicate nature point-by-point (for which a more sophisticated model subject to much longer runs is needed) but rather point out the dynamical importance of a sudden change in the coastline slant (i.e., a kink). We begin by noting that simulations of the no-kink model with "averaged" slant for SIF ($35 - -40^\circ$) lead to sub-critical regime of shedding for $\alpha > 0.15$ but critical or super-critical regime for the more realistic values of $\alpha \leq 0.15$. Therefore, the applicability of this no-kink model is poor. Moreover, the curves for $\alpha = 0.1$ intersect at $\gamma \approx 35^\circ$, implying that, the "no-kink" model is invalid in such conditions because, according to it, the BE cannot grow in the retroreflection area. Hence,

Retroreflection from a double slanted coastline for Agulhas leakage variability

V. Zharkov et al.

Title Page

Abstract

Introduction

Conclusions

References

Tables

Figures



Back

Close

Full Screen / Esc

Printer-friendly Version

Interactive Discussion



we suggest that our Concave I model describes the behavior of Agulhas retroflection better and (Fig. 2) we take γ to be 15° for NPR and 60° for SIF. For the most common cases we estimated the ratios of shedding parameters for both SIF and NPR (Table 1). It is seen that, the intensity of ring shedding significantly decreases during SIF. Therefore, the mass transport from the Indian Ocean to the SA is weaker during SIF than during NPR (despite the non-critical regime in both cases). It is interesting to note that the parameter ratios given in Table 1 almost do not depend on α .

We tried to fit the geometry to nature and make the horizontal scales as close as possible to their real values (see Fig. 2). For this purpose, we adopted Concave II for NPR and Concave III for SIF. The SIF shedding regime near point *C* (Fig. 2) is shown in Fig. 8 for weak vorticity and shallow depth. For a comparison, the NPR shedding regime with the retroflection near point *B* is shown in Fig. 9, where, for clarity, we moved the strongly slanted section out of the figure. (Otherwise, the area of our numerically simulated retroflection shifts gradually to Concave III, meaning a restoration of the SIF regime.) The generation period is less than that shown in Fig. 8 because, although the first two eddies are generated almost at the same time in both figures, the third one lags noticeably behind them in Fig. 8 but does not in Fig. 9. Also, the rings' radii look greater in Fig. 9, implying that the leakage during NPR increases. We note also that, for stronger vorticity and greater upper layer thickness, the results are not that different.

For an initialized α of 1.0, we obtained 123 (with a mean square deviation, MSD, of 40.2) and 93 (with MSD of 20.5) days for SIF and NPR simulations, respectively. The ratio is 1.32, which is greater than our theoretical value of 1.06 (MSD is 0.36). For α of 0.4, the averaged SIF and NPR periods were 118 (with MSD of 43.9) and 110 (with MSD of 18.1) days; the ratio is 1.07 (MSD is 0.31), which is very close to the theoretical value mentioned above. Unfortunately, in our simulations for α of 0.1, the eddy very quickly collapsed due to the relative high importance of viscosity, and the averaged periods could be estimated only with relative errors of 60%. The obtained values were 120 (with MSD 71.9) days for SIF and 145 (with MSD 75.3) days for NPR, so the ratio is 0.83, and the MSD is 0.47. It should be noted, however, that such a variability of

Retroflection from a double slanted coastline for Agulhas leakage variability

V. Zharkov et al.

[Title Page](#)[Abstract](#)[Introduction](#)[Conclusions](#)[References](#)[Tables](#)[Figures](#)[Back](#)[Close](#)[Full Screen / Esc](#)[Printer-friendly Version](#)[Interactive Discussion](#)

Retroflection from a double slanted coastline for Agulhas leakage variability

V. Zharkov et al.

Title Page

Abstract

Introduction

Conclusions

References

Tables

Figures

⏪

⏩

◀

▶

Back

Close

Full Screen / Esc

Printer-friendly Version

Interactive Discussion

averaged values was caused by viscosity rather than by different initialization of α . This is because, during numerical runs, the eddies' PV was strongly altered by viscosity, so that the averaged values of α were about 0.20–0.25 for all the numerics. We note also that the averaged eddies' radii shown in Figs. 8 and 9 are about 180 and 220 km, so their ratio is 0.82, which is somewhat smaller than our theoretical value of 0.96. This is probably again an effect of viscosity because the thickness of large rings (Fig. 9) is not greater than those of the rings in Fig. 8. Therefore, the ratio of the volume fluxes is expected to be comparable to our theoretical value of 0.77. Overall, the numerical simulations confirm the results of our theoretical modeling (Fig. 10). Also, the mean radii and shedding periods for SIF in our numerics are close to those in animation created by the GFDL Oceans and Climate group (see <http://www.gfdl.noaa.gov/oceans-and-climate>): 8 rings shed during 995 days.

We can also compare the ratio of the volume fluxes Φ with observational data, assuming that the ratio of mass transport carried to the SA by rings is not far from the ratio of the entire Agulhas leakages, i.e., the ratio of fluxes carried by filaments does not strongly differ from the ratio of the rings mass flux. According to VS (their Fig. 1), the average ratio of Agulhas leakage to AC transport (T_{AL}/T_{AC}) is $19.2/60.5=0.317$ when the retroflection is protruded westward and $14.2/67=0.212$ when is protruded eastward. The “ratio of these ratios” is 0.67 (confidence range is approximately between 0.61 and 0.75) which is somewhat less than our predicted value of $\Phi_{SIF}/\Phi_{NPR}=0.77$. This could be due to stronger dissipation occurring during the rings longer journey from the eastern retroflection area to the SA than from the western. Note that the ZNb model with $\gamma=60^\circ$ for SIF (and $\gamma=15^\circ$ for NPR) would lead to much worse results: the considered ratio would change from about 0.4–0.6 for $\alpha=1$ to zero for α of less than 0.2 (which is closer to real conditions). Using the data from Fig. 5 (bottom panels) and taking into account that rings carry usually about 70% of the entire leakage, we conclude that, for the experiments by VS, α was between 0.065 and 0.13. Even for the “average” value of the coastal slant (say, $\gamma=37.5^\circ$), the agreement of no-kink model with experimental data for natural values of α poor (Fig. 11). In this figure, we plotted the “ratio of

Φ s” versus α for the kink and no-kink (ZNb) models, as well as the confidence region for the data from VS. It is seen that the curve for the kink model almost touches the confidence area, whereas the no-kink curve goes to zero. (The range of α where the “ratio of Φ s” is zero corresponds to super-critical case when the leakage is shut down).

Finally, using a “ratio of Φ s” of 0.77 and keeping in mind that the ratio of incoming fluxes for SIF and NPR is 1.10–1.15, we conclude that the ratio of outflows is about 0.85–0.90, implying that the kinked coastline plays a defining role in the anti-correlation between the incoming Agulhas flux and leakage to the SA.

7 Summary and conclusions

To begin with, we considered a coastline consisting of two straight sections, one of which is slanted and the other zonal. (This case is referred to as Concave I, see Figs. 2 and 3.) We developed a non-linear model with which we examined the dependency of ring formation, radii, and their detachment period, on the slant angle, the PV of the formed eddies, and the thickness of the undisturbed upper layer. In contrast to the no-kink conclusion of ZNb, there are no critical slant angles in the Concave I case (Figs. 4–5). Rather, when the slant of the non-zonal coastal section is close to 90° , the shedding regime is almost critical, i.e., the shedding is weak but it is not arrested. To confirm or reject this, we carried out numerical simulations that are in fair agreement with those predicted by our model (Figs. 6–7).

To bring our calculations still closer to reality we also considered Concave II (NPR) and Concave III (SIF) where the coastline geometry satisfactorily fits both the actual geography (Fig. 2), and the position of the vanishing WSC. We see (Figs. 8–9) that the intensity of eddies shedding decreased during SIF compared to NPR. Therefore, the mass flux going into rings noticeably weakens during SIF, which is in fair agreement with our theoretical results (Fig. 11). Moreover, both theoretical and numerical results confirm that, when the Agulhas retroflection protrudes eastward, the ratio Φ decreases sufficiently strongly (becoming about 77% of the same ratio for NPR) to explain

Retroflection from a double slanted coastline for Agulhas leakage variability

V. Zharkov et al.

Title Page

Abstract

Introduction

Conclusions

References

Tables

Figures

⏪

⏩

◀

▶

Back

Close

Full Screen / Esc

Printer-friendly Version

Interactive Discussion



Retroflection from a double slanted coastline for Agulhas leakage variability

V. Zharkov et al.

[Title Page](#)[Abstract](#)[Introduction](#)[Conclusions](#)[References](#)[Tables](#)[Figures](#)[Back](#)[Close](#)[Full Screen / Esc](#)[Printer-friendly Version](#)[Interactive Discussion](#)

the anti-correlation between the incoming flux and the leakage to the SA. Indeed, the observed ratio of incoming fluxes for SIF and NPR is 1.10–1.15; therefore, the ratio of outflows is about 0.85–0.90. On the whole, a comparison of our results with VS (Fig. 11) suggests that our model is consistent with the observed anti-correlation between the AC transport and Agulhas leakage. Using the earlier ZNb model instead of the new kink model presented here would lead to significantly worse results for leakage via eddies because even the averaged value of the slant near the point of retroflection becomes super-critical (Fig. 11).

Even though the southern AC is steered by the shelf break rather than the coastline (Lutjeharms, 2006), we neglected the varying bathymetry. This simplification is justified because when the retroflection occurs not far from the concavity of the coastline, the shelf break and coastline are parallel. Also, rings shed from the eastward-shifted retroflection propagate westward and avoid the southern part of the Agulhas Bank because its scale is smaller than the scale of one separated eddy.

The kink model is successfully applied to the case of a weak La-Niña (1986–1987), for which, as we showed, the error in fitting the observational data of mass flux going into eddies is on average 3–4 times less than in the no-kink model simulations. However, it is possible that, as noted by van Sebille (2009), the no-kink model could be better applied to the strong La-Niña events like the early Agulhas retroflection observed in 2000–2001 (see also, de Ruijter et al., 2004), because the eddies shedding was short during this period. One possible explanation is that, during this early retroflection, the AC was strongly interacting with dipoles in the Mozambique Basin. This could result in an AC detachment where the coastline slant does not (yet) change significantly. In view of Pichevin et al. (2009), we expect the no-kink model to be preferable when the AC detaches from the coast somewhere in between East London and Durban. We leave these questions, however, for future investigations.

Acknowledgements. The study was supported by the NASA Doctral Fellowship Grant NNG05GP65H; LANL/IGPP Grant (1815); NSF (OCE-0752225, OCE-9911342, OCE-0545204, OCE-0241036), BSF(2006296), and NASA (NNX07AL97G). V. Zharkov was also

funded by the Jim and Shelia O'Brien Graduate Fellowship. We are grateful to Steve van Gorder for helping in the numerical simulations, to Donna Samaan for helping in preparation of manuscript, and to J. Beal for helping in improving the style.

References

- 5 Arruda, W. Z., Nof, D., and O'Brien, J. J.: Does the Ulleung eddy owe its existence to β and nonlinearities?, *Deep-Sea Res.*, 51, 2073–2090, 2004.
- Biastoch, A., Böning, C. W., and Lutjeharms, J. R. E.: Agulhas leakage dynamics affects decadal variability in Atlantic overturning circulation, *Nature*, 456, 489–492, 2008.
- 10 Bleck, R. and Boudra, D.: Wind-driven spin-up in eddy resolving ocean models formulated in isopycnic and isobaric coordinates, *J. Geophys. Res.*, 91, 7611–7621, 1986.
- Boudra, D. B. and Chassignet, E. P.: Dynamics of the Agulhas retroflection and ring formation in a numerical model, I. The vorticity balance, *J. Phys. Oceanogr.*, 18, 280–303, 1988.
- Byrne, A. D., Gordon, A. L., and Haxby, W. F.: Agulhas eddies: A synoptic view using geosat ERM data, *J. Phys. Oceanogr.*, 25, 902–917, 1995.
- 15 Chassignet, E. P. and Boudra, D. B.: Dynamics of the Agulhas retroflection and ring formation in a numerical model, II. Energetics and ring formation, *J. Phys. Oceanogr.*, 18, 304–319, 1988.
- De Ruijter, W. P. M.: Asymptotic analysis of the Agulhas and Brazil Current systems, *J. Phys. Oceanogr.*, 12, 361–373, 1982.
- 20 De Ruijter, W. P. M., Biastoch, A., Drijfhout, S. S., Lutjeharms, J. R. E., Matano, R. P., Pichevin, T., van Leeuwen, P. J., and Weijer, W.: Indian-Atlantic interocean exchange: Dynamics, estimation and impact, *J. Geophys. Res.*, 104, 20885–20910, 1999.
- De Ruijter, W. P. M. and Boudra, D. B.: The wind-driven circulation in the South Atlantic – Indian Ocean, I. Numerical experiments in a one-layer model, *Deep-Sea Res.*, 32, 557–574, 1985.
- 25 De Ruijter, W. P. M., van Aken, H. M., Beier, E. J., Lutjeharms, J. R. E., Matano, R. P., and Schouten, M. W.: Eddies and dipoles around South Madagascar: formation, pathways and large-scale impact, *Deep-Sea Res.*, 51, 383–400, 2004.
- Esper, O., Versteegh, G. J. M., Zonneveld, K. A. F., and Willems, H.: A palynological reconstruction of the Agulhas Retroflection (South Atlantic Ocean) during the Late Quaternary, *Global Planet. Change*, 41, 31–62, 2004.
- 30

Retroflection from a double slanted coastline for Agulhas leakage variability

V. Zharkov et al.

Title Page

Abstract

Introduction

Conclusions

References

Tables

Figures



Back

Close

Full Screen / Esc

Printer-friendly Version

Interactive Discussion



Retroflection from a double slanted coastline for Agulhas leakage variability

V. Zharkov et al.

[Title Page](#)
[Abstract](#)
[Introduction](#)
[Conclusions](#)
[References](#)
[Tables](#)
[Figures](#)
[⏪](#)
[⏩](#)
[◀](#)
[▶](#)
[Back](#)
[Close](#)
[Full Screen / Esc](#)
[Printer-friendly Version](#)
[Interactive Discussion](#)


- Field, A., Toole, J., and Wilson, D.: Seasonal circulation in the South Indian Ocean, *Geophys. Res. Lett.*, 24, 2773–2776, 1997.
- Goni, G. J., Garzoli, S. L., Roubicek, A. J., Olson, D. B., and Brown, O. B.: Agulhas ring dynamics from TOPEX/POSEIDON satellite altimeter data, *J. Mar. Res.*, 55, 861–883, 1997.
- 5 Gordon, A. L., Lutjeharms, J. R. E., and Gründlingh, M. L.: Stratification and circulation at the Agulhas Retroflection., *Deep-Sea Res.*, 34, 565–599, 1987.
- Lutjeharms, J. R. E.: *The Agulhas Current*, Springer-Verlag, Berlin – Heidelberg – New York, XIV, 330 p., 2006.
- Lutjeharms, J. R. E. and van Ballegooyen, R. C.: Topographic control in the Agulhas Current system, *Deep-Sea Res.*, 31, 1321–1337, 1984.
- 10 Lutjeharms, J. R. E. and van Ballegooyen, R. C.: The retroflection of the Agulhas Current, *J. Phys. Oceanogr.*, 18, 1570–1583, 1988a.
- Lutjeharms, J. R. E. and van Ballegooyen, R. C.: Anomalous upstream retroflection in the Agulhas current, *Science*, 240(n4860), 1770–1772, 1988b.
- 15 Matano, R. P., Simionato, C. G., De Ruijter, W. P. M., Van Leeuwen, P. J., Strub, P. T., Chelton, D. B., and Schlax, M. G.: Seasonal variability in the Agulhas Retroflection region, *Geophys. Res. Lett.*, 25, 4361–4364, 1998.
- Nof, D.: On the β -induced movement of isolated baroclinic eddies, *J. Phys. Oceanogr.*, 11, 1662–1672, 1981.
- 20 Nof, D.: On the migration of isolated eddies with application to Gulf stream rings, *J. Mar. Res.*, 31, 399–425, 1983.
- Nof, D.: The momentum imbalance paradox revisited, *J. Phys. Oceanogr.*, 35, 1928–1939, 2005.
- Nof, D. and Pichevin, T.: The retroflection paradox, *J. Phys. Oceanogr.*, 26, 2344–2358, 1996.
- 25 Nof, D. and Pichevin, T.: The ballooning of outflows, *J. Phys. Oceanogr.*, 31, 3045–3058, 2001.
- Orlanski, I.: A simple boundary condition for unbounded hyperbolic flows, *J. Comput. Phys.*, 21, 251–269, 1976.
- Ou, H. W. and de Ruijter, W. P. M.: Separation of an internal boundary current from a curved coast line, *J. Phys. Oceanogr.*, 16, 280–289, 1986.
- 30 Pichevin, T., Nof, D., and Lutjeharms, J. R. E.: Why are there Agulhas Rings?, *J. Phys. Oceanogr.*, 29, 693–707, 1999.
- Pichevin, T., Herbert, S., and Floc'h, F.: Eddy formation and shedding in a separating boundary current, *J. Phys. Oceanogr.*, 39, 1921–1934, 2009.

Retroflexion from a double slanted coastline for Agulhas leakage variability

V. Zharkov et al.

Title Page

Abstract

Introduction

Conclusions

References

Tables

Figures

⏪

⏩

◀

▶

Back

Close

Full Screen / Esc

Printer-friendly Version

Interactive Discussion

- Quarty, G. D. and Srokosz, M. A.: SST Observations of the Agulhas and East Madagascar Retroflexions by the TRMM Microwave Imager, *J. Phys. Oceanogr.*, 32, 1585–1592, 2002.
- Reason, C. J. C., Lutjeharms, J. R. E., Hermes, J., Biastoch, A., and Roman, R. E.: Inter-ocean fluxes south of Africa in an eddy-permitting model, *Deep-Sea Res. Pt. II*, 50, 281–298, 2003.
- 5 Schouten, M. W., de Ruijter, W. P. M., van Leeuwen, P. J., and Lutjeharms, J. R. E.: Translation, decay and splitting of Agulhas rings in the south-eastern Atlantic ocean, *J. Geophys. Res.*, 105, 21913–21925, 2000.
- Shannon, L. V.: The Benguela ecosystem: Part I. Evolution of the Benguela, physical features and processes, *Oceanogr. Mar. Biol.*, 23, 105–182, 1985.
- 10 Shannon, L. V., Agenbag, J. J., Walker, N. D., and Lutjeharms, J. R. E.: A major perturbation in the Agulhas retroflexion area in 1986, *Deep-Sea Res.*, 37, 493–512, 1990.
- Van Aken, H. M., van Veldhoven, A. K., Veth, C., de Ruijter, W. P. M., van Leeuwen, P. J., Drijfhout, S. S., Whittle, C. P., and Rouault, M.: Observations of a young Agulhas ring, Astrid, during MARE in March 2000, *Deep-Sea Res.*, 50, 167–195, 2003.
- 15 Van Sebille, E.: Assessing Agulhas leakage, Proefschrift ter verkrijging van de graad van doctor aan de Universiteit Utrecht, 165 pp., 2009.
- Van Sebille, E., Biastoch, A., van Leeuwen, P. J., and de Ruijter, W. P. M.: A weaker Agulhas current leads to more Agulhas leakage, *Geophys. Res. Lett.*, 36, L03601, doi:10.1029/2008GL036614, 2009a.
- 20 Van Sebille, E., Barron, C. N., Biastoch, A., van Leeuwen, P. J., Vossepoel, F. C., and de Ruijter, W. P. M.: Relating Agulhas leakage to the Agulhas Current retroflexion location, *Ocean Sci.*, 5, 511–521, 2009b.
- Weijer, W., de Ruijter, W. P. M., Dijkstra, H. A., and van Leeuwen, P. J.: Impact of interbasin exchange on the Atlantic Overturning Circulation, *J. Phys. Oceanogr.*, 29, 2266–2284, 1999.
- 25 Weijer, W., De Ruijter, W. P. M., Sterl, A., and Drijfhout, S. S.: Response of the Atlantic overturning circulation to South Atlantic sources of buoyancy, *Global Planet. Change*, 34, 293–311, 2002.
- Zharkov, V. and Nof, D.: Retroflexion from slanted coastlines – circumventing the “vorticity paradox”, *Ocean Sci.*, 4, 293–306, 2008a.
- 30 Zharkov, V. and Nof, D.: Agulhas ring injection into the South Atlantic during glacials and interglacials, *Ocean Sci.*, 4, 223–237, 2008b.

Retroflection from a double slanted coastline for Agulhas leakage variability

V. Zharkov et al.

Table 1. Theoretically estimated ratios as a function of α .

| α | 0.1 | 0.2 | 0.4 | 0.6 | 0.8 | 1.0 |
|---|------|------|------|------|------|------|
| $\frac{\text{Eddy radius for SIF}}{\text{Eddy radius for NPR}}$ | 0.96 | 0.96 | 0.96 | 0.96 | 0.96 | 0.96 |
| $\frac{\text{Shedding period for SIF}}{\text{Shedding period for NPR}}$ | 1.04 | 1.05 | 1.06 | 1.06 | 1.06 | 1.06 |
| $\frac{\text{Eddy velocity for SIF}}{\text{Eddy velocity for NPR}}$ | 0.93 | 0.92 | 0.91 | 0.91 | 0.91 | 0.90 |

Title Page

Abstract

Introduction

Conclusions

References

Tables

Figures

⏪

⏩

◀

▶

Back

Close

Full Screen / Esc

Printer-friendly Version

Interactive Discussion

Table A1. List of symbols.

| | |
|------------------|--|
| AC | Agulhas Current |
| BE | basic eddy |
| C_x | eddy migration rate in the zonal direction |
| C_y | eddy migration rate in the meridional direction |
| C_{xf} | eddy migration rate after detachment |
| C_{x1}, C_{xu} | values of C_{xf} for eddies with radii R_{fl}, R_{fu} , respectively |
| d | distance between consecutive eddies |
| d_1 | width of incoming current |
| d_2 | width of retroflected current |
| f | the Coriolis parameter |
| f_0 | approximate absolute value of f at the eddy center |
| g' | reduced gravity |
| H | upper layer thickness outside the retroflexion area |
| h | upper layer thickness |
| h_0 | upper layer thickness at the wall |
| \tilde{h} | upper layer thickness in the stagnant wedge situated between the incoming and retroflected currents, to be distinguished from H , which is the thickness outside the retroflexion region |
| MOC | meridional overturning circulation |
| NPR | normal position of retroflexion |
| PV | potential vorticity |
| Q | mass flux of the incoming current |
| q | mass flux of the retroflected current |
| R | radius of the eddy (a function of time) |
| R_f | radius of the eddy at the moment of detachment |
| R_{fl}, R_{fu} | “lower” and “upper” boundaries of R_f |
| SIF | strong incoming flux |
| Sv | Sverdrup ($10^6 \text{ m}^3 \text{ s}^{-1}$) |
| t | time |
| t_f | period of eddies generation |

Retroflexion from a double slanted coastline for Agulhas leakage variability

V. Zharkov et al.

Title Page

Abstract Introduction

Conclusions References

Tables Figures

⏪ ⏩

◀ ▶

Back Close

Full Screen / Esc

Printer-friendly Version

Interactive Discussion



Retroflection from a double slanted coastline for Agulhas leakage variability

V. Zharkov et al.

Table A1. Continued.

| | |
|----------------------|--|
| t_{fl}, t_{fu} | “lower” and “upper” boundaries of t_f |
| VS | van Sebille et al. (2009a, b) |
| WSC | wind stress curl |
| x, y | zonal and meridional coordinate axes in the moving system |
| ZNa | Zharkov and Nof (2008a) |
| ZNb | Zharkov and Nof (2008b) |
| α | vorticity coefficient (twice the Rossby number) |
| β | meridional gradient of the Coriolis parameter |
| γ | slant of the “eastern” section of coastline |
| δ_1, δ_2 | differences between the eddy radius and current widths d_1, d_2 , respectively |
| $\Delta\rho$ | difference between densities of lower and upper layer |
| ν | viscosity (in numerics) |
| ρ | upper layer density |
| Φ | ratio of mass flux going into eddies and incoming mass flux |
| Φ_l, Φ_u | values of Φ for eddies with radii R_{fl}, R_{fu} , respectively |
| ρ | upper layer density |
| Φ | ratio of mass flux going into eddies and incoming mass flux |
| Φ_l, Φ_u | values of Φ for eddies with radii R_{fl}, R_{fu} , respectively |

Title Page

Abstract

Introduction

Conclusions

References

Tables

Figures

◀

▶

◀

▶

Back

Close

Full Screen / Esc

Printer-friendly Version

Interactive Discussion

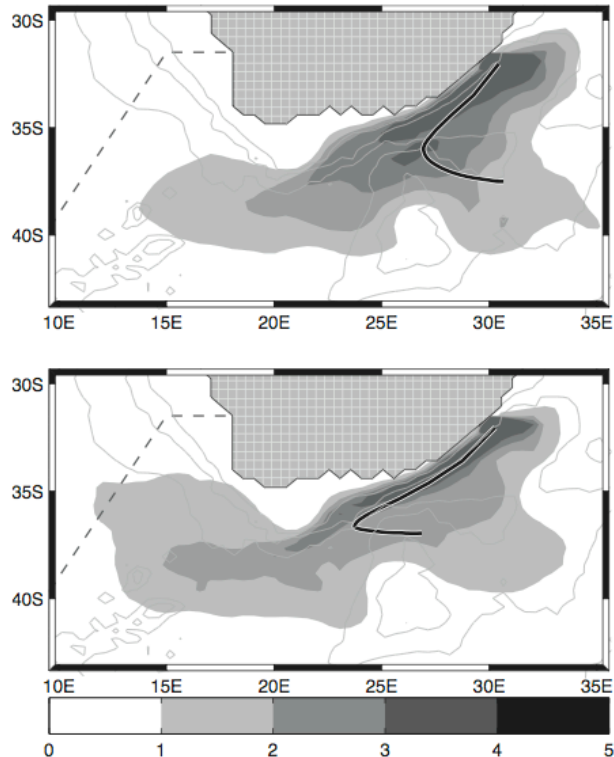


Fig. 1. The transport density (filled shaded patches, in Sv) based on floats distribution. Upper panel: The first six months after release of all floats in 1986–1987, when the transport of the AC (TAC, hereafter) was 65.4 Sv. Lower panel: The same but for 1988–1989, TAC=61.0 Sv. The thick black lines are the transport mean trajectories. The bathymetry is shown as gray lines (1500 m contour interval). For lower TAC (lower panel), the current detaches from the continental slope farther downstream. The retroflexion is, consequently, moved westward and the magnitude of Agulhas leakage is increased. Adapted from van Sebille (2009).

Retroflexion from a double slanted coastline for Agulhas leakage variability

V. Zharkov et al.

Title Page

Abstract Introduction

Conclusions References

Tables Figures

⏪ ⏩

◀ ▶

Back Close

Full Screen / Esc

Printer-friendly Version

Interactive Discussion

Retroflexion from a double slanted coastline for Agulhas leakage variability

V. Zharkov et al.

Title Page

Abstract

Introduction

Conclusions

References

Tables

Figures

⏪

⏩

◀

▶

Back

Close

Full Screen / Esc

Printer-friendly Version

Interactive Discussion

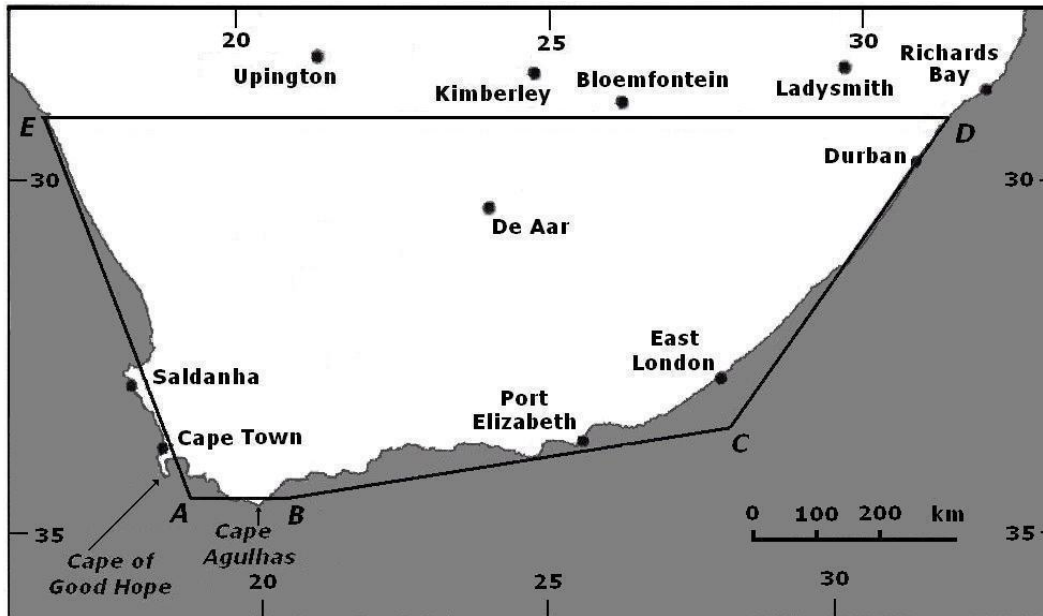


Fig. 2. Map of South Africa with a superimposed pentagon showing the used simplifications. ABC corresponds to Concave II (NPR), BCD to Concave III (SIF), and when the section BC is shrunk to zero, the remaining ABCD corresponds to Concave I (mixture of NPR and SIF).

Retroflection from a double slanted coastline for Agulhas leakage variability

V. Zharkov et al.

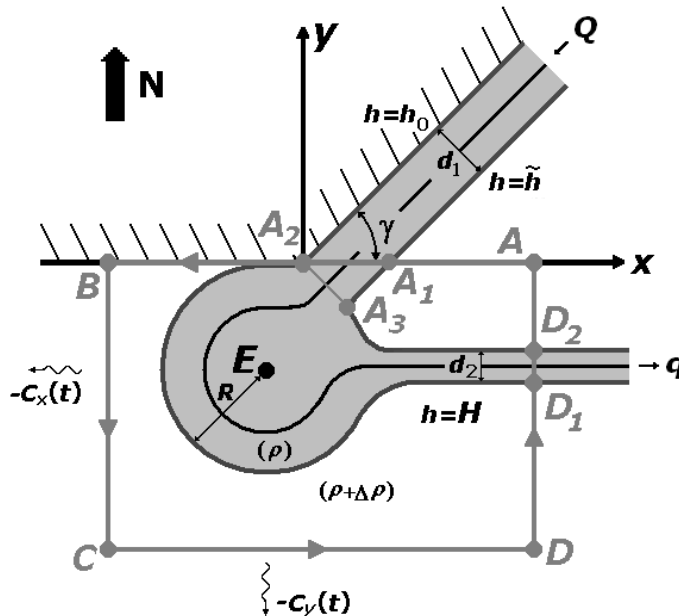


Fig. 3. A schematic diagram of the Concave I model under study. E is the center of the base eddy (BE). The incoming flux Q flows along the wall whereas the outgoing (retroflected) flux q is directed to the east. The widths of the currents are d_1 and d_2 , respectively. The “wiggly” arrow indicates the migration of the base eddy (BE); this migration results from both the eddy growth, which forces the eddy away from the zonal wall, and from β , which forces the eddy along this wall. We shall see that the migration $-C_y(t)$ is primarily due to the growth, whereas $-C_x(t)$ is primarily due to β . The thick grey line (with arrows) indicates the integration path, $ABCD A$; \tilde{h} is the upper layer thickness of the stagnant region wedged in between the upstream and retroflecting current, and H is the off-shore thickness. It is important to realize that the ring forms downstream of A_2 and immediately starts migrating westward. Consequently, the integrated momentum flux along the slanted wall involves an unknown force acting on the wall (and, therefore, cannot be used) but the zonal integrated momentum does not.

| | |
|--------------------------|--------------|
| Title Page | |
| Abstract | Introduction |
| Conclusions | References |
| Tables | Figures |
| ◀ | ▶ |
| ◀ | ▶ |
| Back | Close |
| Full Screen / Esc | |
| Printer-friendly Version | |
| Interactive Discussion | |



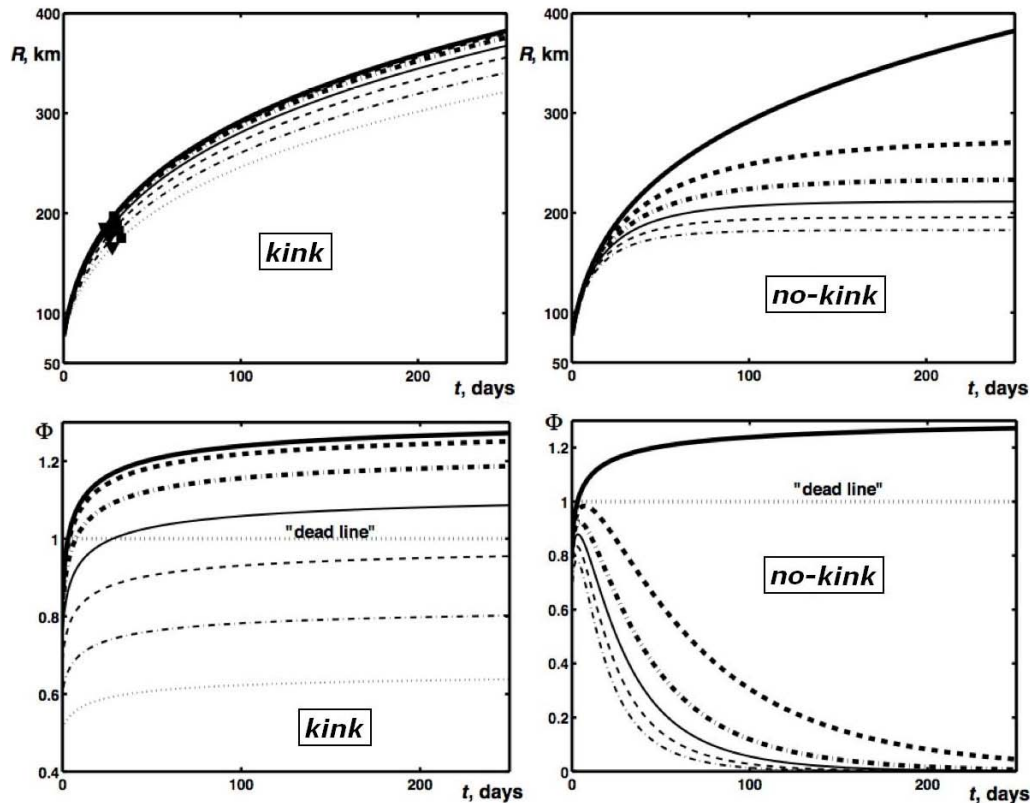


Fig. 4. Concave I BE radius (upper left panel) and Φ , the mass flux ratio (lower left panel), versus time for $\gamma=0^\circ$ (solid thick line), 15° (dashed thick line), 30° (dash-and-dotted thick line), 45° (solid thin line), 60° (dashed thin line), 75° (dash-and-dotted thin line), and 90° (dotted thin line). The straight dotted dead line (lower left panel) show the limit of $q=0$, $\Phi=1$. Triangles and squares denote the lower and upper boundaries of the detachment period for $\beta=2.3 \times 10^{-11} \text{ m}^{-1} \text{ s}^{-1}$, $\alpha=1$, $h_0=300$. The panels on the right show the analogous plots for the no-kink ZNa model.

Retroflection from a double slanted coastline for Agulhas leakage variability

V. Zharkov et al.

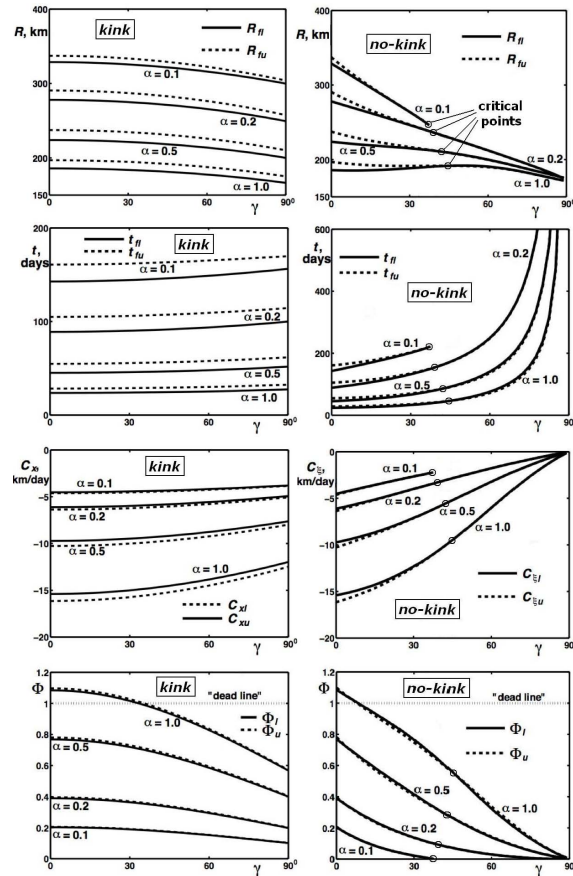


Fig. 5. From top to bottom: plots of R_{ll} and R_{lu} , t_{ll} and t_{lu} , C_{xi} and C_{xu} , Φ_l and Φ_u against γ for Concave I with $h_0=300$ m, and $\beta=2.3 \times 10^{-11} \text{ m}^{-1} \text{ s}^{-1}$. The curves are paired, where solid and dashed lines show the lower and upper boundaries of the eddy radius, respectively. Each pair of curves is marked by a corresponding value of α . In the left panels, the upper and lower boundaries do not intersect. The right panels, on the other hand, shows the plots for ZNB model, where the upper and lower boundaries do intersect, implying the existence of critical slant angles. Such critical points are circled.

[Title Page](#)
[Abstract](#)
[Introduction](#)
[Conclusions](#)
[References](#)
[Tables](#)
[Figures](#)
[◀](#)
[▶](#)
[◀](#)
[▶](#)
[Back](#)
[Close](#)
[Full Screen / Esc](#)
[Printer-friendly Version](#)
[Interactive Discussion](#)

Retroflection from a double slanted coastline for Agulhas leakage variability

V. Zharkov et al.

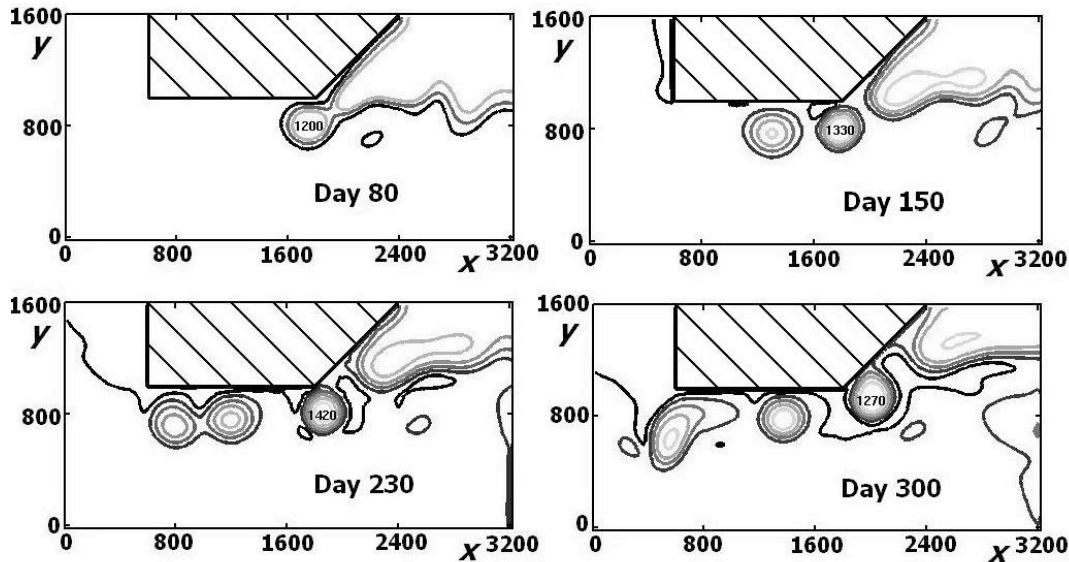


Fig. 6. Thicknesses for Concave I with a small kink and high upstream vorticity experiment ($\gamma=45^\circ$, $\alpha=1$, $h_0=300$ m, and $\nu=700$ m² s⁻¹). Here, the eastern wall is not critically sloped so rings are formed upstream of the kink. This figure, as well as Fig. 7, is given here merely to illustrate the dynamics – the outflow latitude is the same in both figures and they are not necessarily associated with either the SIF or NPR, whose numerical runs are displayed in Figs. 8 and 9. Thicknesses are given in meters, and the x and y scales are in kilometers. Note that we used $\beta=6\times 10^{-11}$ m⁻¹ s⁻¹. Note that experiments with rings closer to each other (shown in Figs. 8 and 9) required higher viscosity for stability because of the higher shear.

Title Page

Abstract

Introduction

Conclusions

References

Tables

Figures

◀

▶

◀

▶

Back

Close

Full Screen / Esc

Printer-friendly Version

Interactive Discussion



Retroflection from a double slanted coastline for Agulhas leakage variability

V. Zharkov et al.

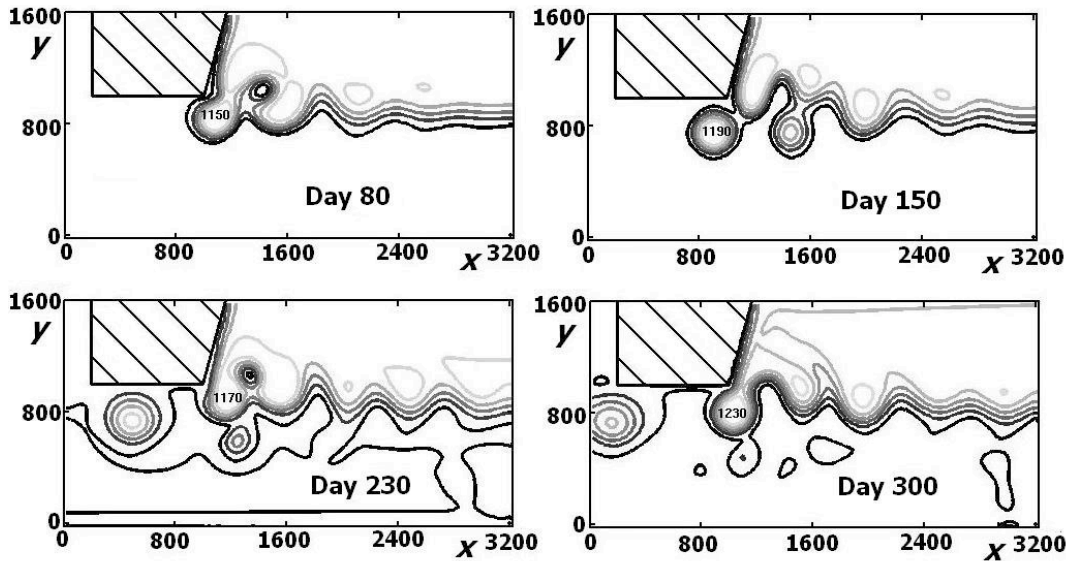


Fig. 7. The same as in Fig. 6, but for a large kink and weak vorticity (Concave I, $\gamma=75^\circ$, $\alpha=0.4$, $h_0=300$ m, and $\nu=700$ m² s⁻¹). Here, the eastern wall slant is too high to produce rings, so rings are produced just downstream of the kink, which effectively locks the position of the retroflection. Only one eddy is detached, and the second is about to be detached after 300-th day of simulation. Note that the viscosity here is the same as in its counterpart example shown in Fig. 6.

[Title Page](#)
[Abstract](#)
[Introduction](#)
[Conclusions](#)
[References](#)
[Tables](#)
[Figures](#)
[⏪](#)
[⏩](#)
[◀](#)
[▶](#)
[Back](#)
[Close](#)
[Full Screen / Esc](#)
[Printer-friendly Version](#)
[Interactive Discussion](#)

Retroflection from a double slanted coastline for Agulhas leakage variability

V. Zharkov et al.

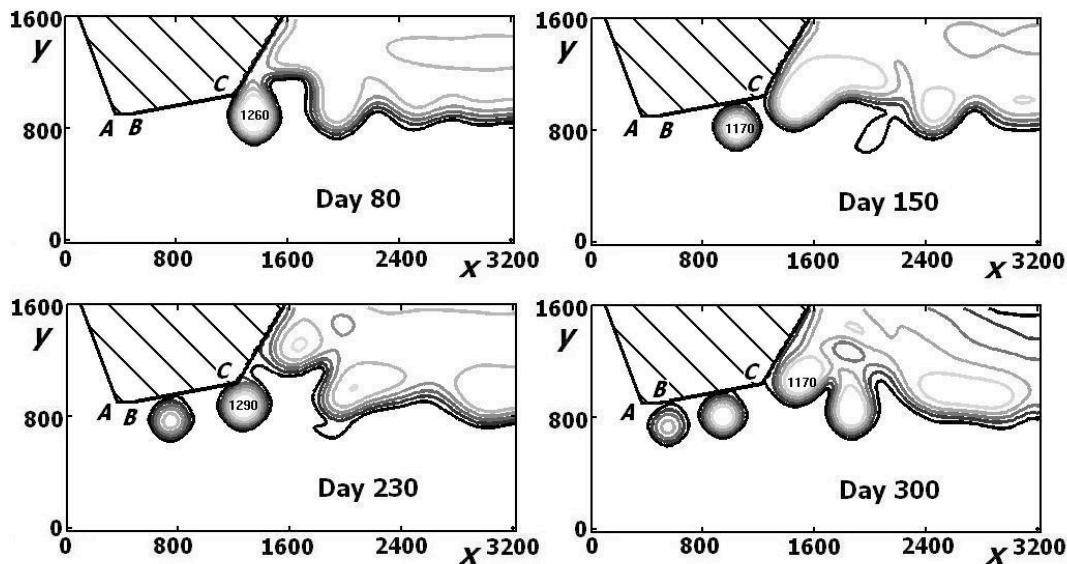


Fig. 8. Upper layer thicknesses during SIF, where a weak vorticity current retroflects near the kink situated in between the slightly and strongly slanted coastlines (Concave III, $\alpha=0.4$, $h_0=0$, and $\nu=1000 \text{ m}^2 \text{ s}^{-1}$).

Title Page

Abstract

Introduction

Conclusions

References

Tables

Figures

⏪

⏩

◀

▶

Back

Close

Full Screen / Esc

Printer-friendly Version

Interactive Discussion

Retroflection from a double slanted coastline for Agulhas leakage variability

V. Zharkov et al.

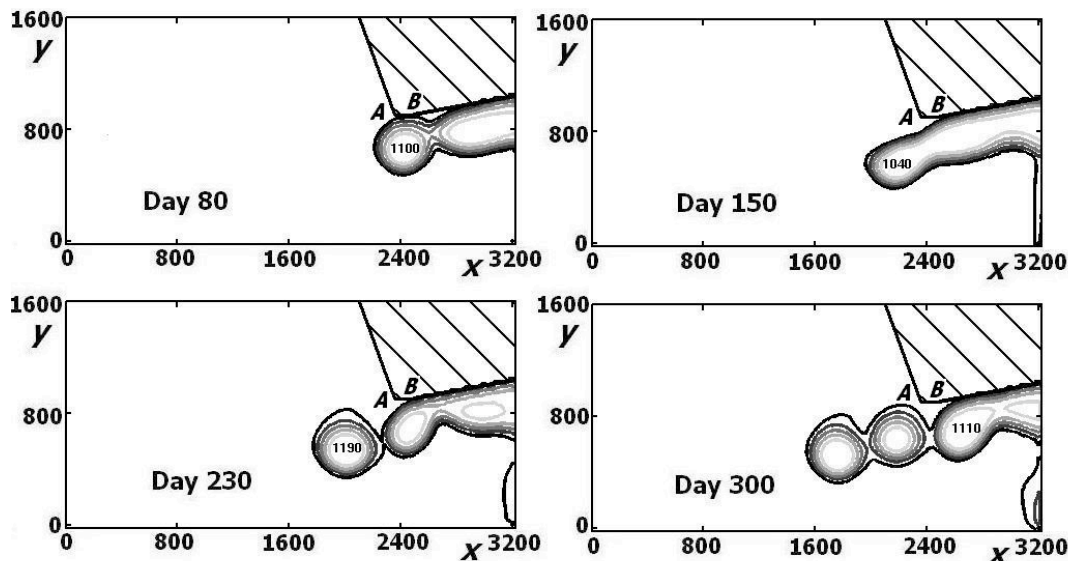


Fig. 9. Upper layer thicknesses during NPR (Concave II) for numerical simulation of the weak vorticity current retroflecting near the termination of slightly slanted coastline (near the Cape Agulhas, Concave II, $\alpha=0.4$, $h_0=0$, and $\nu=1200\text{ m}^2\text{ s}^{-1}$). Rings generation occurs more often than in Fig. 8, and the rings' radii are larger. The shed eddies form a chain, mainly in the open ocean. Note that the retroflection latitude here is to the south of that shown in Fig. 8. Also, to maintain stability, we had to increase the viscosity here by about 20% compared to Fig. 8.

[Title Page](#)
[Abstract](#)
[Introduction](#)
[Conclusions](#)
[References](#)
[Tables](#)
[Figures](#)
[⏪](#)
[⏩](#)
[◀](#)
[▶](#)
[Back](#)
[Close](#)
[Full Screen / Esc](#)
[Printer-friendly Version](#)
[Interactive Discussion](#)

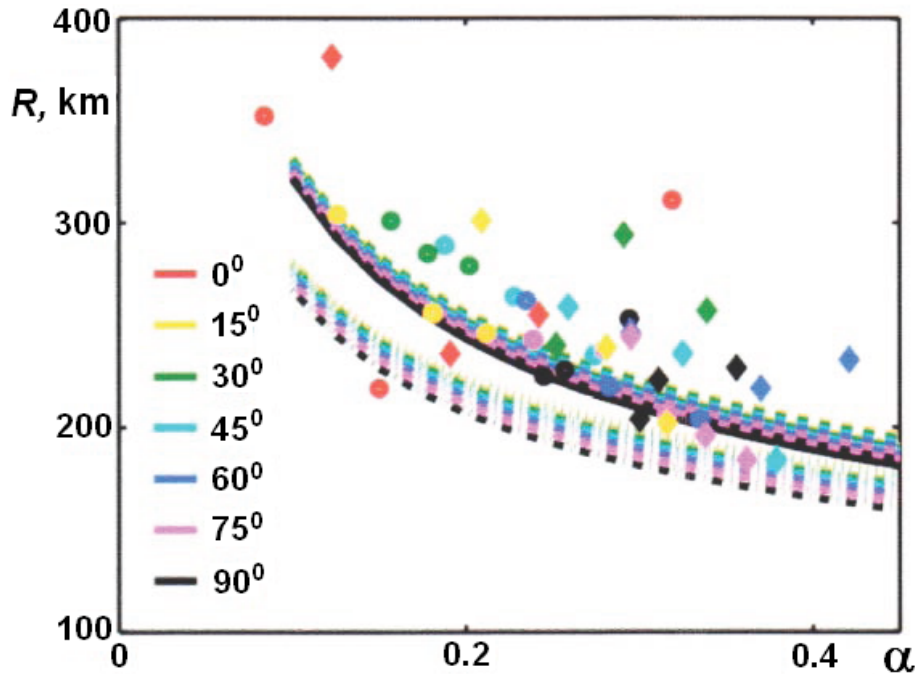


Fig. 10. A comparison of the kink model radii with those of the numerical runs. The eastern wall slant (γ) is shown with in color. The western wall slant is nearly zero. Note that, as in ZNb, α was averaged over the periods of simulations. The numerical radii are larger than in our model because of viscosity, which spins the rings down flattening them out. It is mentioned here in passing that the rings propagation rates are smaller in the numerics than in our model, also due to viscosity.

Retroflection from a double slanted coastline for Agulhas leakage variability

V. Zharkov et al.

| | |
|--------------------------|--------------|
| Title Page | |
| Abstract | Introduction |
| Conclusions | References |
| Tables | Figures |
| ⏪ | ⏩ |
| ⏴ | ⏵ |
| Back | Close |
| Full Screen / Esc | |
| Printer-friendly Version | |
| Interactive Discussion | |



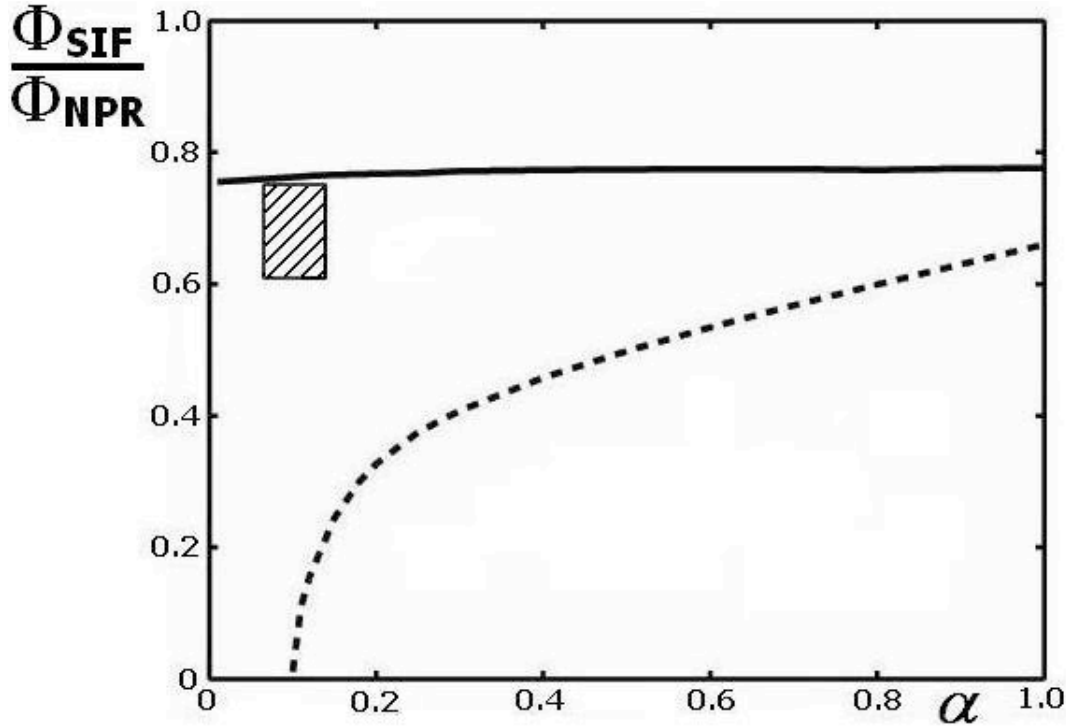


Fig. 11. Analytical calculation of the mass transports ratio Φ for SIF and NPR computed using the “kink” model (solid line) and “no-kink” model (ZNb, with an averaged slant, dashed line). The hatched rectangle shows the confidence area of the data from VS. Clearly, the kinked model is the one to use, not the no-kink one.

Retroflection from a double slanted coastline for Agulhas leakage variability

V. Zharkov et al.

| | |
|--------------------------|--------------|
| Title Page | |
| Abstract | Introduction |
| Conclusions | References |
| Tables | Figures |
| ◀ | ▶ |
| ◀ | ▶ |
| Back | Close |
| Full Screen / Esc | |
| Printer-friendly Version | |
| Interactive Discussion | |

